Toward Objective Quantification of Perfusion-weighted Computed Tomography in Subarachnoid Hemorrhage: Quantification of Symmetry and Automated Delineation of Vascular Territories[1]

Celina Imielinska, PhD, Xin Liu, MD, MS, Joel Rosiene, PhD, Michael E., Sughrue, BS, Ricardo J. Komotar, MD, J. Mocco, MD, Evan R. Ransom, BA, Angela Lignelli, MD, Brad E. Zacharia, BS, E. Sander Connolly, Jr, MD, Anthony L. D'Ambrosio, MD

Rationale and Objectives. Perfusion-weighted computed tomography (CTP) is a relatively recent innovation that estimates a value for cerebral blood flow (CBF) using a series of axial head CT images tracking the time course of a signal from an intravenous contrast bolus.

Materials and Methods. CTP images were obtained using a standard imaging protocol and were analyzed using commercially available software. A novel computer-based method was used for objective quantification of side-to-side asymmetries of CBF values calculated from CTP images.

Results. Our method corrects for the inherent variability of the CTP methodology seen in the subarachnoid hemorrhage (SAH) patient population to potentially aid in the diagnosis of cerebral vasospasm (CVS). This method analyzes and quantifies side-to-side asymmetry of CBF and presents relative differences in a construct termed a Relative Difference Map (RDM). To further automate this process, we have developed a unique methodology that enables a computer to delineate vascular territories within a brain image, regardless of the size and shape of the brain.

Conclusions. While both the quantification of image symmetry using RDMs and the automated assignment of vascular territories were initially designed for the analysis of CTP images, it is likely that they will be useful in a variety of applications.

Key Words . CT; brain; perfusion; cerebral blood flow; aneurysmal subarachnoid hemorrhage; ischemic stroke

Stroke is the third leading cause of death and disability in contemporary society. Subarachnoid hemorrhage (SAH) accounts for approximately 6% to 8% of all strokes and 22% to 25% of cerebrovascular deaths. Between 1 million and 12 million people in the United States harbor intracranial aneurysms, and the annual prevalence of aneurysmal SAH (aSAH) in this country is believed to be in excess of 30,000 persons. Despite considerable advances in the diagnosis and treatment of SAH, the outcome remains poor [1,2]. The presence of subarachnoid blood is sufficient to produce severe luminal narrowing of cerebral arteries. This process is called cerebral vasospasm (CVS). However, the primary mechanism for vasospasm is uncertain, and therefore, any patient with SAH is considered to be at risk

Acad Radiol 2005; 12:874–887

[1] From the Departments of Biomedical Informatics (C.I., X.L.), Computer Science (C.I.), Neurological Surgery (M.S., R.K., J.M., E.R., B.Z., E.S., A.D.) and Neuroradiology (A.L.), Columbia University, New York, NY, USA; and the Department of Mathematics and Computer Science, Eastern Connecticut State University, CT (J.R.) Received March 16, 2005; revision received March 16; revision accepted March 31. Address correspondence to C.I. e-mail: ci42@columbia.edu

doi:10.1016/j.acra.2005.03.074

for developing CVS [3,4]. Rapid diagnosis and treatment of CVS pose a true clinical dilemma, and the lack of reliably predictive tests often leads to delayed intervention and irreversible neurological injury [5]. Developing a noninvasive, reliable, and sensitive test that could risk-stratify patients for CVS during the first days of their hospital admission into high-, medium-, and low-risk populations would be of immense benefit for patients and could potentially decrease health care costs.

Perfusion-weighted computed tomography (CTP) is a relatively recent innovation that utilizes a series of axial head CT images to track the time course of a signal from an administered bolus of intravenous contrast [6,8]. These images are then processed using either deconvolution or maximum slope algorithms to extrapolate a numerical value for cerebral blood flow (CBF) [9,18,19]. While "bolus tracking" methods may provide accurate quantification of CBF under controlled conditions, variability in cardiac function, systemic blood pressure, and cerebrovascular tone often seen in the setting of acute SAH makes quantitative and qualitative assessment of these studies both difficult and potentially hazardous [7–12].

Although CTP has found some utility in the diagnosis and management of ischemic stroke, its potential use in the diagnosis and management of delayed CVS has not been investigated. Furthermore, since this imaging study is both fast and noninvasive, it is an ideal diagnostic test in this unstable patient population. Unfortunately, due to the inherent variability described above, there is no currently accepted, standardized method of interpreting these scans. Most commonly, scans are interpreted using the qualitative detection of gross side-to-side asymmetry of CBF, an approach that lends itself to misdiagnosis and potential failure to treat CVS. Recent work with CTP has focused on the development of methods to quantitatively analyze CTP images. Most of these approaches utilize the region of interest (ROI) method [11,13]. In this approach, the clinician circles an ROI on the post-processed CTP image, and the mean CBF is compared to that of the corresponding ROI in the contralateral hemisphere to detect asymmetry. A growing body of data supports improved safety and efficacy of this approach in the setting of acute ischemic stroke, though data for SAH is less complete.

We have developed a novel algorithm for analyzing post-processed CTP images obtained from a standard perfusion CT software package (Siemens Medical Solutions, Malvern, PA). This method converts CBF values, which must be viewed as meaningless outside of the context of a given scan, to relative "difference," which represents side-to-side asymmetry and is a meaningful value as it is specific to a given scan. This conversion is performed by comparing a small region of the scan to the corresponding region in the contralateral hemisphere, quantifying the degree of relative difference, and representing this quantity of relative difference in 2D and 3D in a construct we termed a Relative Difference Map (RDM). We analyze and quantify the amount of "relative difference" in both brain hemispheres and the 6 major vascular territories to assess the degree of hypoperfusion in the regions. The method is automated and has the potential to provide a better and more stable analysis of the perfusion parameters of SAH patients.

MATERIALS AND METHODS

Patient Population and Image Selection

Between 1996 and 2003, all patients presenting to New York Presbyterian Hospital following SAH resulting from the rupture of an angiographically confirmed intracranial aneurysm were prospectively enrolled in the SAH Outcomes Project (SHOP), an IRB-approved project in which extensive clinical and long-term health outcomes data were collected on all patients.

CTP studies were performed by the treating physicians as part of routine management. During a 2-year period (July 2001 to July 2003), 122 CTP scans were performed in 85 patients in SHOP. Digital Imaging and Communications in Medicine (DICOM) images from these patients were collected retrospectively, processed by a neuroradiologist, and selected for this analysis. Unusable scans were excluded on the basis of having poor tissue enhancement curves. All images of SAH patients were taken from this cohort.

Based on the assumptions described below, we excluded patients with significant midline shift from focal hematoma, hydrocephalus, or focal cerebral edema. Future work will focus on automatically identifying the midline in a curvilinear fashion to correct for possible structural asymmetries.

Premises and Assumptions

For our analysis, we made the following assumptions: (1) In normal cases, the axial CT images of the left and right hemispheres are structurally symmetric and compa-

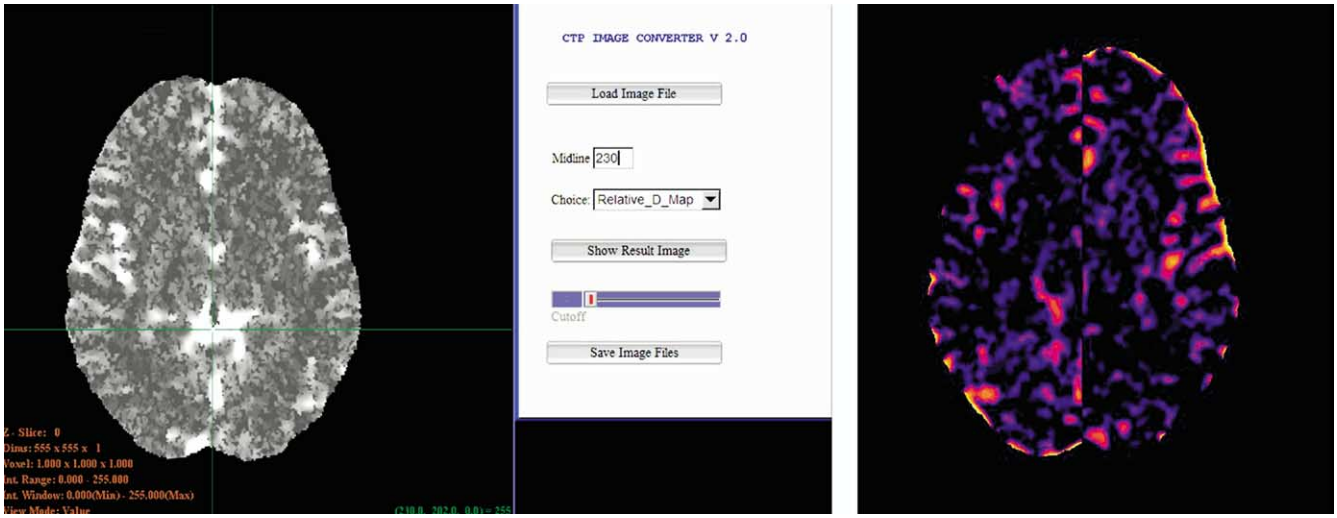

Figure 1. Relative difference map for CBF: **(a)** CBF image displayed by Siemens' perfusion software; **(b)** CT input CBF with selected midline, **(c)** output RDM.

rable, and there should be no more than minor side-to-side differences in relative blood flow between the 2 hemispheres; (2) In abnormal cases, the left and right hemispheres are still structurally symmetric and comparable, but there is a significant relative blood flow difference between the 2 hemispheres; this can be detected using CTP images.

Preliminary Work: The Relative Difference Map (RDM) as a Measure of Asymmetry

Original color DICOM images (Fig. 1a) were transformed into 8-bit binary format, where the color scales in the original images are normalized into the scale ranging from 0 to 255 (Fig. 1b). Using our stated assumptions, a straight line representing the image midline (an axis of symmetry) was drawn by hand along the anterior–posterior axis through the septum pelucidum to equally divide the brain into 2 symmetric hemispheres. For quantification of symmetry 2 9 x 9 windows are constructed in both brain hemispheres that visit the opposite regions pixel-by-pixel in a scan-line fashion. Centered at a pixel location at its 9 x 9 window is compared to its sister window in the opposite hemisphere, around the constructed axis of symmetry. The Kolmogorov-Smirnov test [14] is applied to find the greatest statistical discrepancy between the observed and expected cumulative frequencies between 2 populations. The average intensities of pixels in the window from one hemisphere are subtracted from those of the contralateral hemisphere, and the absolute difference is divided by the intensity value on the side where CBF reading is relatively larger ("relatively normal hemisphere"). The result is displayed on the side where the reading of the mirrored window is smaller ("relatively abnormal hemisphere") to display the score for relative difference map (Fig. 1c). While the data in this figure utilizes CBF data, an identical method can be used to quantify the cerebral blood volume (CBV), and an inverse method can be used to quantify the time to peak (TTP) parameter.

The resulting RDM is then subdivided by hand into the 6 major cerebrovascular territories, and regional histograms are calculated for each territory. Figure 2 represents a hypothetical distribution of histograms of regions in the RDMs computed for CBF. These curves represent the conceptual basis behind our algorithm. We hypothesize that in disease states, "difference" will cluster in af-

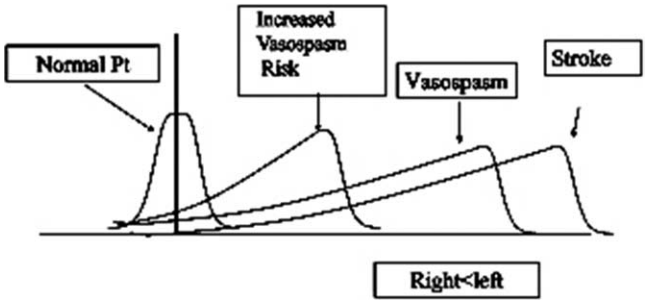

Figure 2. Hypothesized regional histograms quantified from relative difference maps (RDM) of normal patients; patients with increased vasospasm risk; angiographic vasospasm; and ischemic stroke.

fected territories, and will skew the regional histogram to the right in "problem areas."

Toward a Fully Automated System for Quantification of CTP

While our original method appeared promising, its dependence on a significant degree of user input limited its potential in that it was entirely dependent on subjective determination of the axis of symmetry and delineation of cerebrovascular territories. Thus, minor intra-observer variations could potentially cause significant alteration in the data provided by RDMs. As well, the method was very time consuming and not feasible to use in a clinical setting.

Thus, we sought to develop a methodology by which RDMs could be generated with minimal user input. This presented a particular challenge in the SAH population as CTPs were obtained from brains of differing sizes and shapes, with varying degrees of minor distortion of cortical surface anatomy caused by extracerebral masses, specifically postoperative pneumocephalus, or small amounts of subarachnoid blood. While such blood and air can be segmented out and do not appear in the postprocessed image, minor distortions of brain shape are very common in the SAH population and present a special difficulty in our attempt to design automated systems for assessing symmetry.

The method described herein addresses this problem and can be roughly summarized in 4 key steps:

(a) Computation of axis of symmetry of an input CBF image and re-orientation of the image in upright position, if necessary.
(b) Computation of unwrapped image.
(c) Computation of RDM using the assigned axis of symmetry and 9 x 9 window difference calculation on the unwrapped image. Resampling of data back onto the original dataset.
(d) Registration of 6 vascular territories using generic angles and computation of a histogram for each territory.

Automated Determination of the Axis of Symmetry

Computation of axis of symmetry in an irregular 2D image is a multistep process which we perform in this method using the following processes: (a) computation of the convex hull of the anatomical region (ie, an outline of a brain region); (b) computation of centroids from which the axis of symmetry is derived; (c) unwrapping of the image onto a rectangular stretcher with the axis of symmetry as a vertical midline, to potentially calibrate selection of the axis using underlying image information.

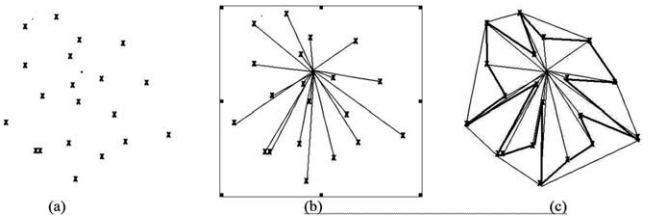

Figure 3. Computation of convex hull (CH) from a set of points in 2D: **(a)** input, **(b)** sorting, **(c)** star-shaped polygon and its convex hull.

Computation of the Convex Hull

A 2D region is convex if a line segment between any 2 points in the region is inside that region. A convex hull of a 2D shape is the smallest convex region that fully encloses the shape. There are standard techniques to compute a convex hull for a set of points in 2D by first constructing a star-shaped polygon [15] as illustrated in Figure 3. Because our images consist of digital pixels, we first devised a method that can sweep a 2D digital image from a centroid point by visiting each pixel and generating a star-shaped polygon that allows quick and easy computation of the convex hull.

Computation of Fourier Shape Descriptor Using Ray Casting: Determination of Bounding Functions of Theta

For a given 2D digital image, to obtain a boundary function for a region in the image described by points on the outermost edge of the region, we cast rays from the centroid (c_x,c_y) of the region outward at specific increasing angles, θ. To obtain a valid sampling, we increased theta at each step by a $\Delta\theta < \sin^{-1}\left(\frac{1}{2R_{\max}}\right)$ as indicated in Figure 4, some rays may pass through a singularity in the boundary, meaning that it is possible that a ray will pass between 2 boundary pixels that are diagonally connected. To prevent this we can make the ray have a thickness on the order of the precision of the machine (Fig. 5).

By recording the length of the ray at each angle, we have a description of a bounding function $R(\theta)$ of the region as a function of θ. This function may not have desirable properties; for example, it may not be convex.The

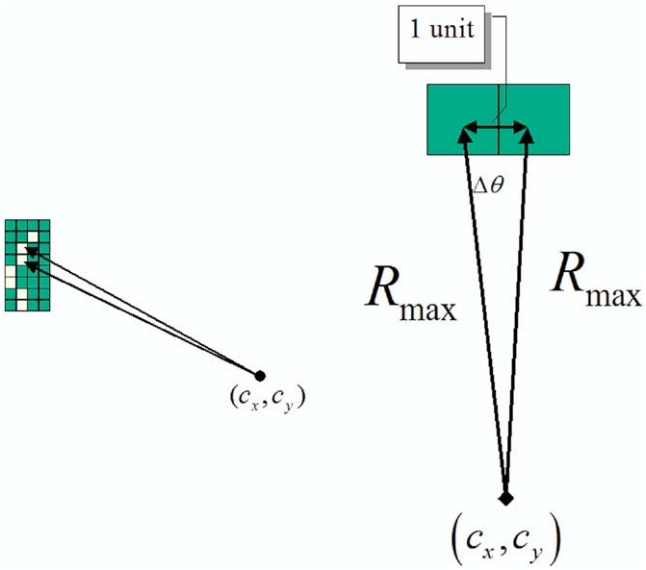

Figure 4. The casting of rays, and the angle step size relative to the maximum ray length.

convex hull of the boundary can be obtained with the points on the convex hull still being parameterized by theta. By linearly interpolating the radii between 2 points on the convex hull, it is possible to obtain a "blob" which shares points with the convex hull but smoothly varies from one point to the next. (It may not be convex, but "nearly"-convex, Fig. 6).

This function provides an easy means of determining if a point within a distance of R_{max} of the centroid is inside or outside of the region enclosed by the bounding function. We need only calculate the angle and compare the 2 distances obtained: the distance of the point under consideration; and the radius obtained from $R(\theta)$.

Having this periodic bounding function allows calculation of the Fourier shape descriptors (FSD) [16], of the bounding function (region) and calculate the centroids of any angular section of the object, and derive axes of symmetry as shown in Figure 7.

Image Unwrapping

The FDS of the shape allows us to unwrap the corresponding boundaries of the original image and the "blob" over the angle θ, and this new representation allows for multiple manipulations of the original image. For example, image unwrapping allows us to compare the distance between 2 boundaries.

Following unwrapping, we can view each 2D image in a dual representation: original and unwrapped. The

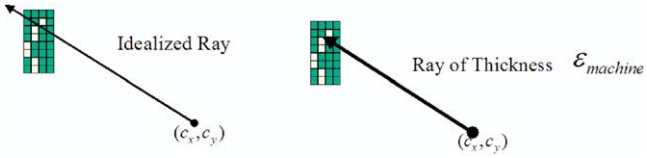

Figure 5. To prevent a ray passing between 2 diagonally connected boundary pixels we increase the ray by the machine's precision.

unwrapped image can be used for (a) selection and calibration of axis of symmetry (Fig. 8a); (b) the comparison of analogous portions of the brain to compute a relative difference map (Fig. 9); (c) interactive removal and selection of regions from the center of the image; and (d) selection of generic angles that are used to approximate the 6 cerebrovascular territories in the brain, as shown in Figure 8b.

Moreover, after the data is unwrapped, each of the radii can be renormalized to equal length, to facilitate the comparison of features in the left and right halves of the image. The stretched image provides a registration of the left and right data that allows the direct comparison of relevant points in the original image. In addition, a window may be applied prior to the "unwrapping" and "stretching" to compensate for anatomical differences in the dataset and errors in the selection of the axis of symmetry. After the completion of relevant operations performed on the "stretched" image, the results are resampled back into the same shape as the "original" dataset. When multiple pixels would map to the same point, the results may be averaged, or the maximum taken to create a composite element.

Computation of Plane of Axis of Symmetry in a CTP Image

To exploit symmetry, we automatically align the image along an axis of symmetry and create the left-to-right test that highlights discrepancies in the dataset. We automatically generate 2 types of axes of symmetry for

(a) Symmetry of content. The axis of symmetry that passes through a focal point (eg, a centroid of an anatomical region of interest). Once the convex hull and corresponding Fourier shape descriptor have been computed for a given image, pixel intensities are used to compute the centroids in the image, and derive the axis of symmetry
(b) Symmetry of shape. The axis of symmetry pass-

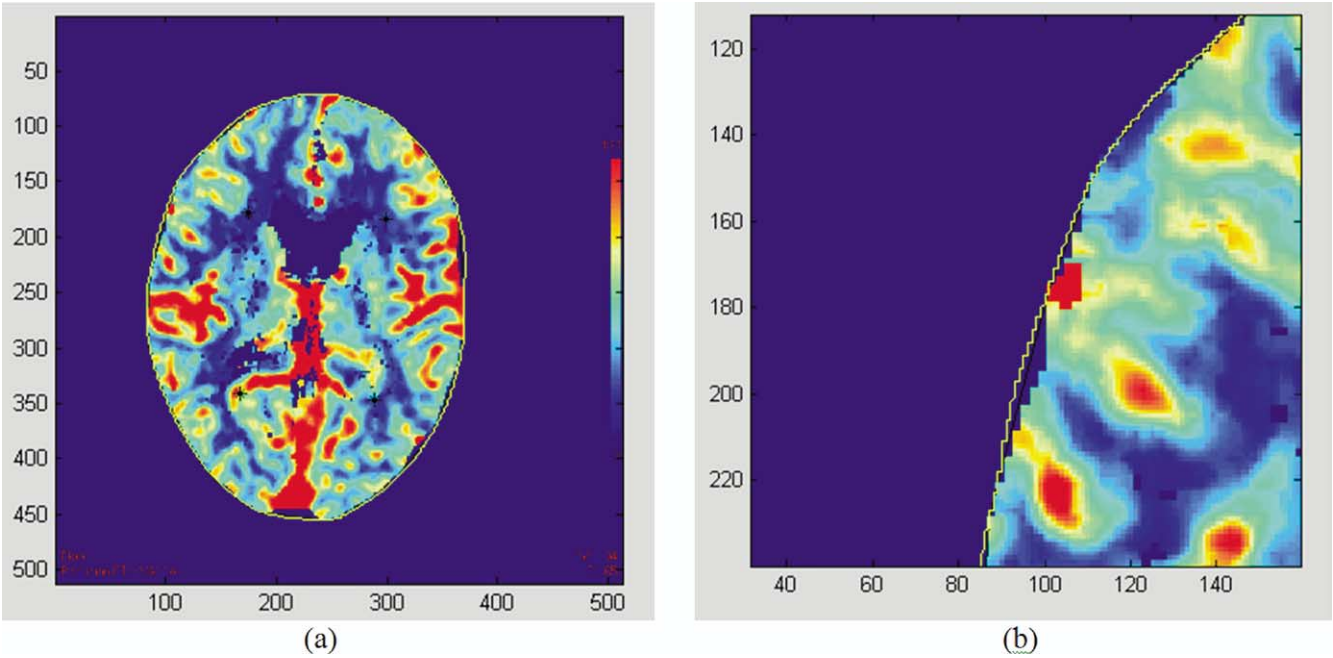

Figure 6. Convex hull and the blob: **(a)** The black line bounding the image is the convex hull, the outermost yellow line is a blob which contains the convex hull, and the black asterisks are the centroids of the 4 quadrants of the blob. **(b)** A closeup view of the convex hull and the blob.

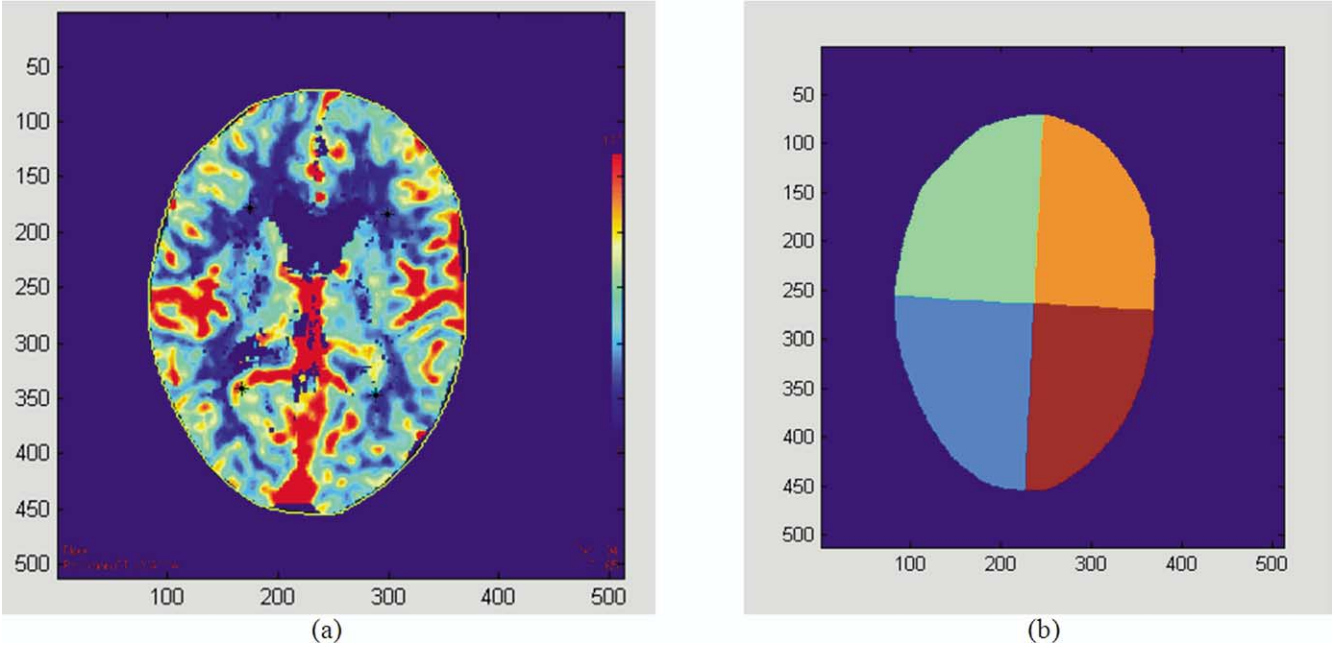

Figure 7. Axis of symmetry: **(a)** An input image and **(b)** 4 quadrants derived from the centroids computed of the blob (FDS) that yield axes of symmetry.

ing through the centroid of the unwrapped dataset. The perfusion-weighted image is unwrapped onto a rectangular stretcher with the axis of symmetry as a vertical line in the middle. The symmetry axis is adjusted by finding the indentation point in the unwrapped stretched image.

While the symmetry of content is useful in other appli-

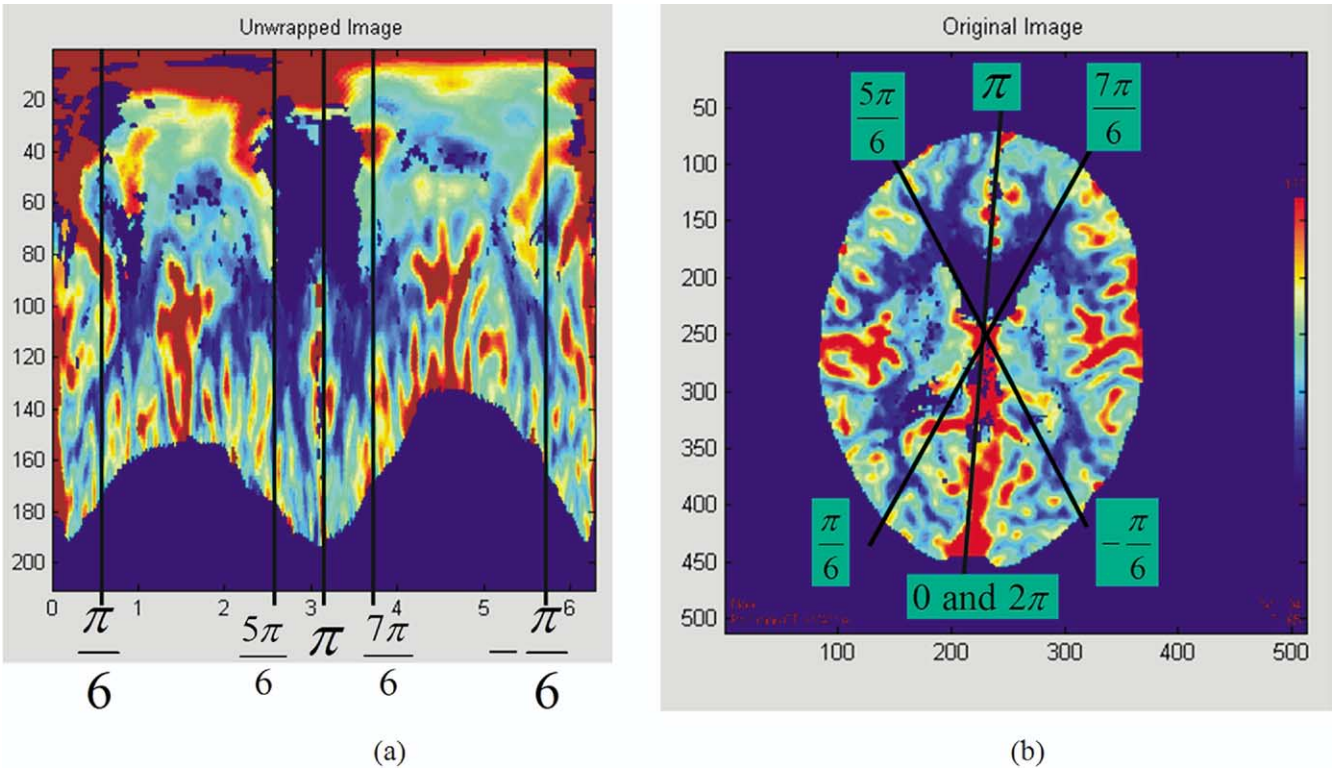

Figure 8. **(a)** The data, unwrapped, by walking from $\theta = 0$ to $\theta = 2\pi$, and from 0 radius to the length of the radii. The vertical bars correspond to lines that partition the image into 6 vascular territories. **(b)** The corresponding input image with 6 vascular territories.

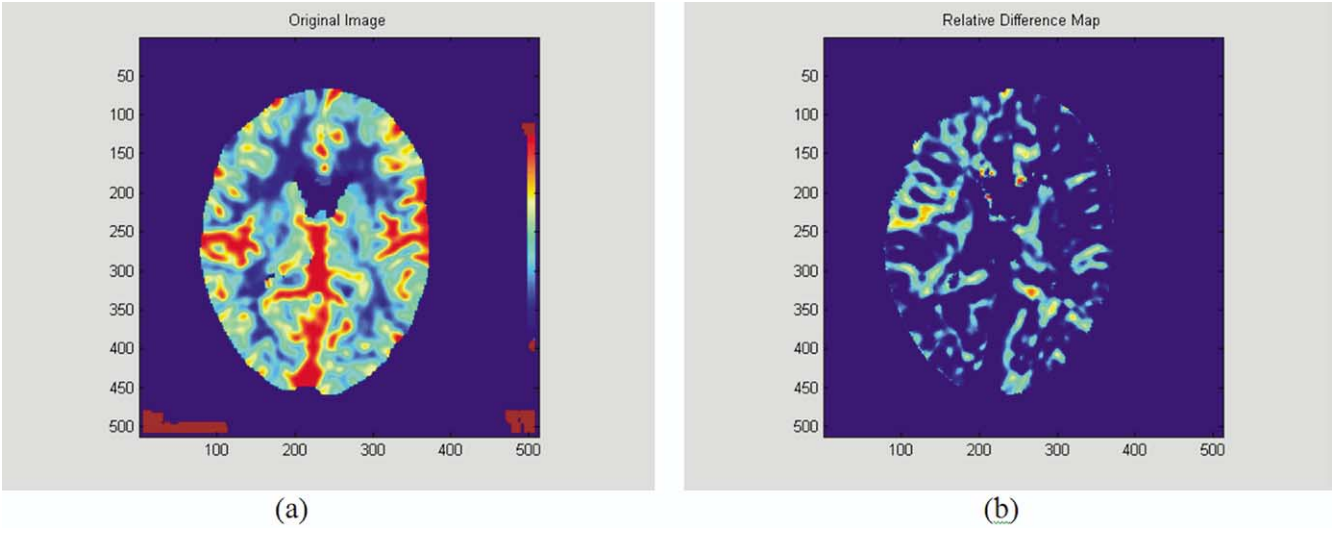

Figure 9. **(a)** The original image processed by a 9 x 9 window, **(b)** The RDM for the image processed on 9 x 9 windows.

cations, in the method presented in this article, we use the symmetry of shape to compute an axis of symmetry in a CBF image as a preprocessing step for computation of the RDM.

Computation of Relative Difference Maps (RDMs)

RDMs are calculated in this automated method, using principles similar to those utilized by the earlier manually aided method [17] with the difference that the axis of

symmetry is computed automatically. Given an input image and its unwrapped representation with the axis of symmetry, we compute the RDM (Fig. 9). From the unwrapped representation of the RDM we derive left and right hemispheres.

Automated Registration of Cerebrovascular Territories.

Because the most relevant application of CBF quantification is the determination of regional CBFs in the 6 major vascular territories of the brain (anterior cerebral artery [ACA], middle cerebral artery [MCA], and posterior cerebral artery [PCA] territories in the left and right hemispheres), we sought to develop an automated method for dividing brain images into these territories so that each region could be analyzed independently. Achieving this task is difficult for 2 principle reasons. First, the territories are irregularly shaped. Second, the territories differ greatly in both shape and size. Since the results of our quantified method are presented as histograms of the RDM values in each of the vascular territories, and the geometric and statistical features of the histograms are to be used for clinical interpretation of patients with SAH, we believe that defining generic, simplified, estimated vascular territories might be a good first approach to automation of the process.

In our preliminary results we delineated the vascular territories using anatomical landmarks that were operator-dependent and time consuming. Because of these inherent limitations to the manual method, we sought to develop a method for automatically dividing the brain tissue into generic vascular territories in a reproducible and reliable way. The advantages of such an automated tool in the clinical setting are obvious, as this is the way the brain is conceptually divided by clinicians treating patients with suspected or known brain ischemia.

In Figure 8 we outline the steps of this method. Briefly, this method uses an unwrapped input CBF image to roughly divide the brain into generic territories using estimated angles that roughly estimate the ACA, MCA, and PCA territories. These sub-divisions are then mapped into a corresponding RDM image. This is achieved (Fig. 8a) by walking from $\theta = 0$ to $\theta = 2\pi$, and from radius 0 to the length of 2 radii, defining vertical bars corresponding to the lines that partition the unwrapped image into 6 vascular territories. The angles that we have found best estimate the territories are: (a) right posterior cerebral artery at $\theta = \left(0, \frac{\pi}{6}\right)$, (b) right middle cerebral artery at $\theta = \left(\frac{\pi}{6}, \frac{5}{6}\pi\right)$, (c) right anterior cerebral artery at $\theta = \left(\frac{5}{6}\pi, \pi\right)$, (d) left anterior cerebral artery at $\theta = \left(\pi, \frac{7}{6}\pi\right)$, (e) left middle cerebral artery at $\theta = \left(\frac{7}{6}\pi, -\frac{\pi}{6}\right)$, (f) right posterior cerebral artery at $\theta = \left(-\frac{\pi}{6}, 0\right)$. When mapped into the original image (Figure 8b), the wedge-shaped vascular territories are defined by these generic angles, and plotting the relative difference values for all the pixels within each territory generates the RDM histogram.

RESULTS

Preliminary Results: RDMs With Manual Demarcation of the Axis of Symmetry and the Vascular Territories

Our preliminary results were encouraging and suggested the potential promise of the RDM method for characterizing asymmetry in CTP images. The 3 illustrative cases described below were selected because they represent the spectrum of potential CBF alterations. The images are presented as RDMs processed from CBF maps. Data for Patient 2 were kindly provided by Dr. Tomandl, Dept. of Neuroradiology, University of Erlangen-Nuremberg.

Patient 1.— The patient is a 43-year-old man who presented with Hunt and Hess grade II SAH. Cerebral angiography disclosed a large (2 cm) MCA aneurysm, which involved the lenticulostriates. The patient's clinical course was unremarkable from a neurological standpoint, with no episodes of CVS detected by daily transcranial Doppler sonography (TCD), cerebral angiography, or routine neurological examination. On SAH day 5, the patient underwent CTP, depicted in Figure 10. Regional histograms of vascular territories demonstrate relatively minimal deviation of the curve from zero in all territories, indicating relatively normal levels of perfusion throughout the brain.

Patient 2.— The patient is a 77-year-old woman who presented with symptoms consistent with left MCA infarction. Figure 11 clearly demonstrates large wedge-shaped region of severe hypoperfusion in the

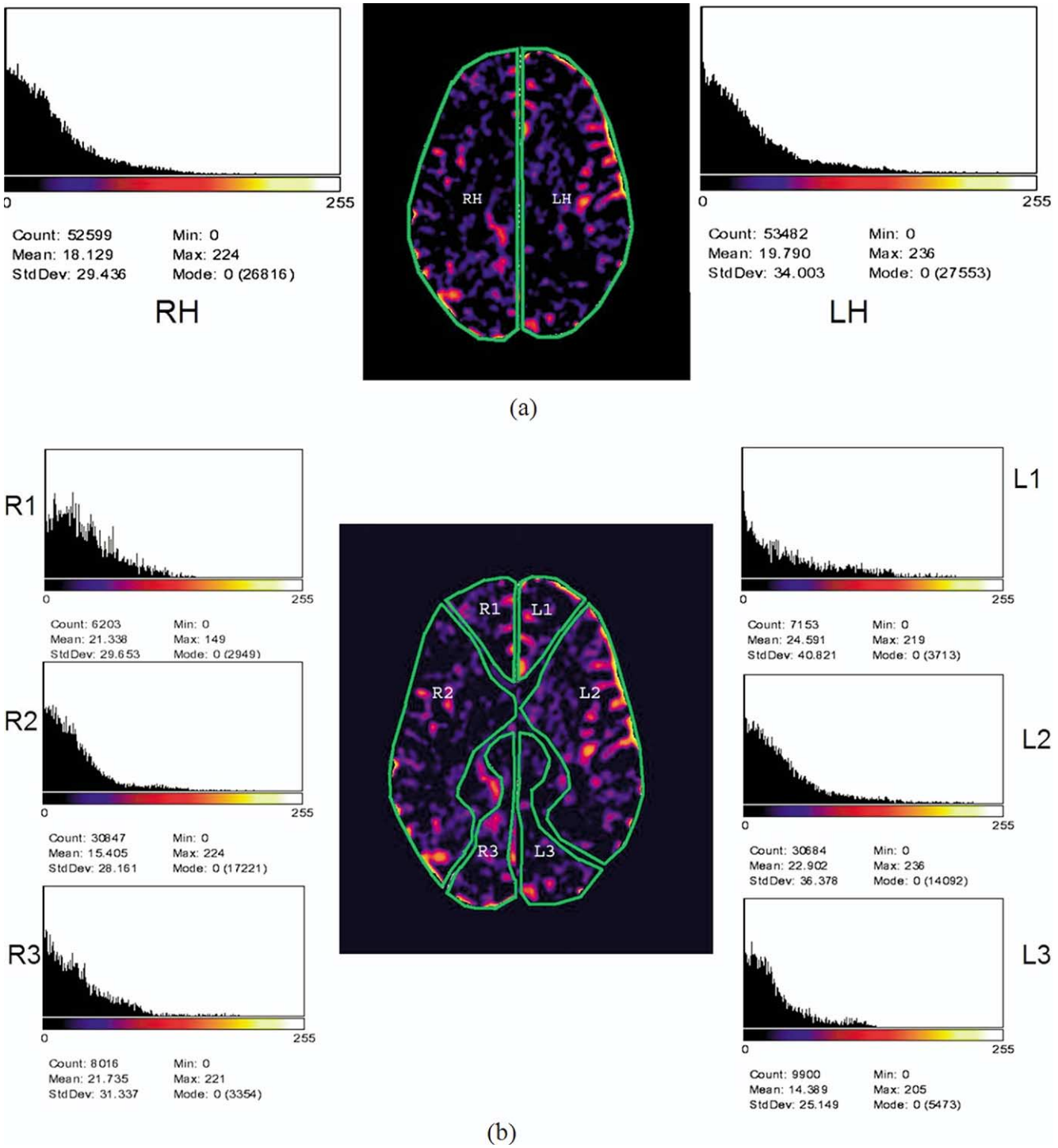

Figure 10. Patient with "normal" CBF": histograms for **(a)** left and right hemispheres, **(b)** 6 vascular territories: L1, left anterior cerebral artery; L2, left middle cerebral artery; L3, left posterior cerebral artery; R1, right anterior cerebral artery; R2, right middle cerebral artery; R3, right posterior cerebral artery.

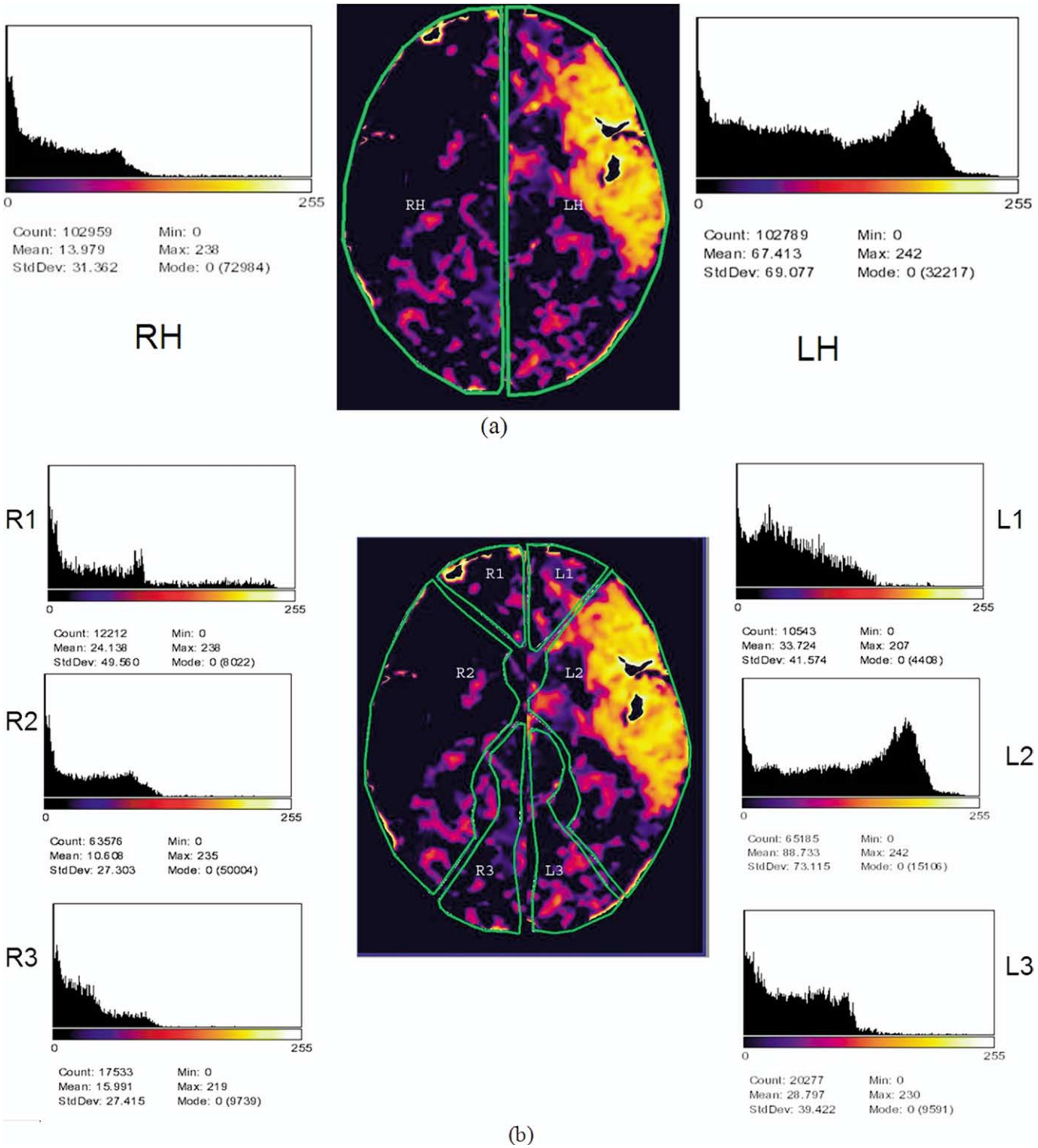

Figure 11. Patient with ischemic stroke: histograms for **(a)** left and right hemispheres, **(b)** 6 vascular territories.

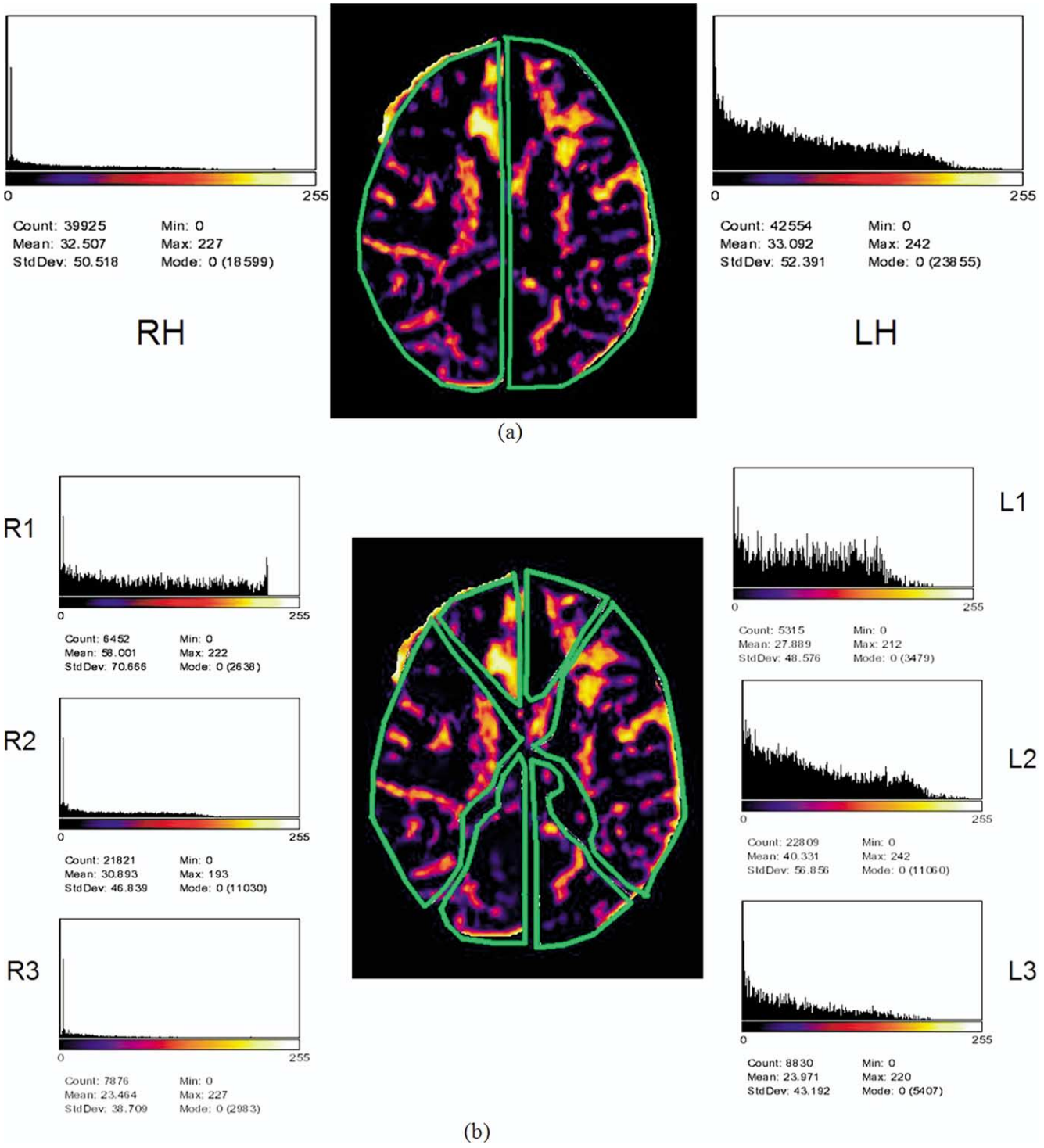

Figure 12. Patient with SAH: histograms for **(a)** left and right hemispheres, **(b)** 6 vascular territories.

MCA territory consistent with acute proximal occlusion of this vessel. When this image was processed using our algorithm, a clear peak on the far right was seen in the histogram representing the left MCA territory that is consistent with our theoretical stroke curve as shown in Figure 2. The histograms for other vascular territories have significantly smaller means, and many appear "normal."

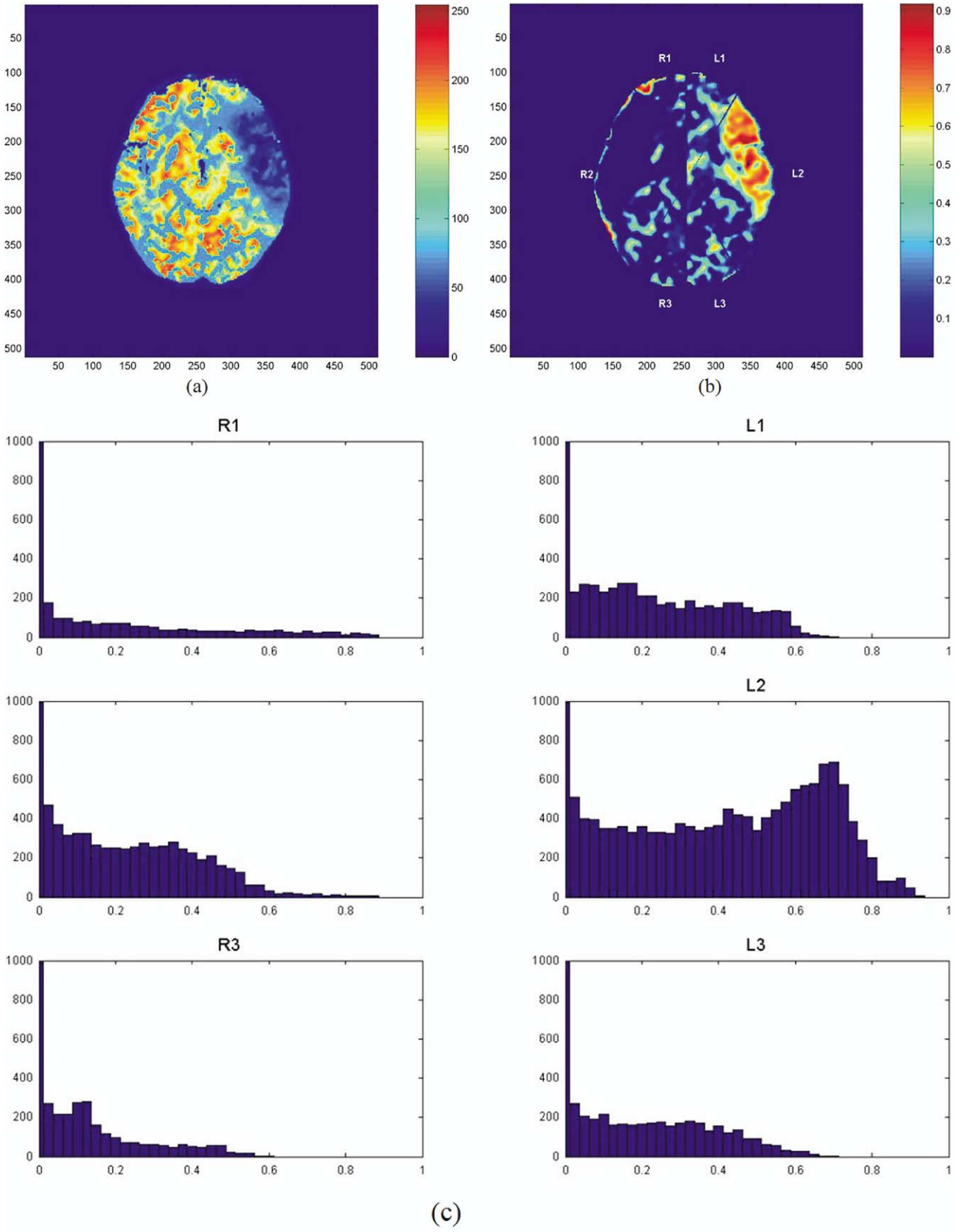

Figure 13. Results with automated RDM/histogram generation: Same patient as shown in Figure 11. The automated system provides similar results as those generated by hand drawing. **(a)** Input CBF image **(b)** RDM with 6 vascular territories **(c)** histograms for 6 vascular territories: L1, left anterior cerebral artery; L2, left middle cerebral artery; L3, left posterior cerebral artery; R1, ranterior cerebral artery; R2, right middle cerebral artery; R3, right posterior cerebral artery.

Patient 3.— Patient is a 36-year-old woman who presented with Hunt and Hess grade IV SAH. Cerebral angiography disclosed a 4-mm x 3-mm right anterior choroidal artery aneurysm. Her neurological examination improved significantly postoperatively. However, on SAH day 5, she experienced an acute decline in mental status, but neurological exam demonstrated no focal neurological deficit. A CTP performed at that time (Fig. 12), was read as normal by an attending neuroradiologist. The patient subsequently developed bilateral arm weakness and was taken for angiography, which revealed severe vasospasm of the right and left MCA and right ACA. This spasm was treated with angioplasty, with significant clinical improvement. Unfortunately, however, follow-up MRI 2 months later demonstrated old cerebral infarction in the right frontal lobe. The RDMs demonstrate significant regions of side-to-side asymmetry in the left MCA and right ACA territories, consistent with the results seen at angiography. The histograms of these regions, while not as striking as those seen for Patient 2, nevertheless demonstrate significant increases in frequency of significantly mismatched pixels (ie, shift of curve to the right).

Subsequent Results With Fully Automated RDM Generation and Vascular Territory Delineation

We have found that RDMs and their histograms derived for vascular territories can be successfully generated using the automated method described above and the results closely approximate those obtained by careful manual delineation. In the histograms shown, we use bucket size (an interval in the x axis of the histogram) of 0.02, and the number of pixels in each bucket is depicted using a normalized scale consistent across all histograms.

In all cases, the automated process produced similar histograms to those obtained by the manual method. For the sake of brevity, we present the results for one patient, Patient 2 (Fig. 13), who at the time of the scan was suffering a large left MCA ischemic stroke. These data closely mimic the results obtained by hand-drawn territories. This demonstrates that this process can be adequately automated to rapidly generate RDM/histogram data of equal quality to those done by a clinician.

DISCUSSION

In this article we describe a novel methodology that aims to provide an objective quantitative measure of side-to-side CBF asymmetry measured by CTP. Our preliminary results have been promising; however, it should be noted that validation of these methods is still in process. Further, while the SAH subjects presented here were young, previously asymptomatic patients who were unlikely to have premorbid intracranial arterial stenoses, our analysis did not include baseline Day 0 imaging analysis. Thus, although unlikely given the clinical history, it is possible that the asymmetries detected could represent premorbid intracranial arterial disease. Currently, we are performing validation studies of our software in a prospective fashion, with emphasis on comparison to baseline scans, to minimize the effect of premorbid cerebrovascular disease.

We implemented a fully automated method for computation of the RDM of postprocessed CT perfusion images and creation of histograms in each vascular territory. We are in the process of designing and implementing an automated system for analyzing histogram features to provide clinicians with a quantitative assessment of CBF quality. However, generating a reliable and reproducible approach to the analysis of postprocessed CT perfusion data will require a long-term effort.

Interestingly, the creation of our algorithm necessitated the development of a number of novel methodologies for addressing specific issues of image processing and analysis that have the potential for use in other medical imaging application. A fundamental pattern of patho-anatomical alteration common to numerous disease processes is the development of side-to-side asymmetry within the organ structure. Consequently, looking for asymmetry is a common method used throughout radiology. While gross, homogenous side-to-side asymmetry probably does not require numerical analysis of image characteristics using a computer, subtler, patchy asymmetry may be missed routinely.

The strength of our method is its emphasis on perfusion asymmetry as the principle manifestation of cerebral ischemia, though this may also be one of its shortcomings. This is particularly true with respect to CVS following SAH. In uncommon cases of widespread exposure of cerebral arteries to subarachnoid blood, CVS may occur bilaterally and thus possibly result in the cancellation of measured perfusion defects. While this is an anticipated limitation of this method, it should be noted that while diffuse multivessel angiographic vasospasm is commonly noted on vasospasm, bilateral vasospasm severe enough to cause cerebral infarction (that would lead to a clinically important cancellation effect) is exceedingly uncommon. Indeed, only 16 cases of bilateral ACA infarction due to vasospasm have been reported in the literature to

date [5], and thus should pose only minimal limitations to the detection of vasospasm using symmetry based methodologies.

Our algorithm provides a robust method for detecting the edges of an organ, determining its axis of symmetry, and characterizing the degree of side-to-side mismatch using regional histograms. While application of these methods to other regions of the body might be limited by a lack of true side-to-side symmetry, the potential applications of a fully developed, automated method for complex characterization and quantification of asymmetry are numerous and span multiple fields of medicine.

REFERENCES

1. Janjua N, Mayer, SA. Cerebral vasospasm after subarachnoid hemorrhage. Curr Opin Crit Care 2003; 9:113–119
2. Ronkainen A, Niskanen M, Rinne J, Koivisto T, Hernesniemi J, Vapalahti M. Evidence for excess long-term mortality after treated subarachnoid hemorrhage. Stroke 2001; 32:2850–2853
3. Weir B. The history of cerebral vasospasm. Neurosurg Clin N Am 1990; 1:265–276
4. Barker FG 2nd, Heros RC. Clinical aspects of vasospasm. Neurosurg Clin N Am 1990; 1:277–288
5. Sanchez RaP-SJ. Radiologic features of cerebral vasospasm. Neurosurg Clin N Am 1990; 1:289–306
6. Axel L. Cerebral blood flow determination by rapid-sequence computed tomography: Theoretical analysis. Radiology. 1980; 137:679–686
7. Roberts HC, Dillon WP, Smith WS. Dynamic CT perfusion to assess the effect of carotid revascularization in chronic cerebral ischemia. AJNR: Am J Neuroradiol 2000; 21:421–425
8. Nabavi DG, Cenic A, Craen RA, et al. CT assessment of cerebral perfusion: Experimental validation and initial clinical experience. Radiology 1999; 213:141–149
9. Ostergaard L, Sorensen AG, Kwong KK, Weisskoff RM, Gyldensted C, Rosen BR. High resolution measurement of cerebral blood flow using intravascular tracer bolus passages. Part II: Experimental comparison and preliminary results. Magn Reson Med 1996; 36:726–736
10. Ostergaard L, Weisskoff RM, Chesler DA, Gyldensted C, Rosen BR. High resolution measurement of cerebral blood flow using intravascular tracer bolus passages. Part I: Mathematical approach and statistical analysis. Magn Reson Med 1996; 36:715–725
11. Koenig M, Kraus M, Theek C, Klotz E, Gehlen W, Heuser L. Quantitative assessment of the ischemic brain by means of perfusion-related parameters derived from perfusion CT. Stroke 2001; 32:431–437
12. Axel L. Tissue mean transit time from dynamic computed tomography by a simple deconvolution technique. Invest Radiol 1983; 18: 94–99
13. Nabavi DG, Kloska SP, Nam E-M, et al. Mosaic: Multimodal stroke assessment using computed tomography: Novel diagnostic approach for the prediction of infarction size and clinical outcome. Stroke 2002; 33: 2819–2826
14. Chakravarti L, and Roy J. Handbook of methods of applied statistics. New York, NY: John Wiley and Sons; 1967.
15. Preparata FP, Shamos MI. Computational geometry. New York: Springer; 1985.
16. Gonzalez RC, Woods RE. Digital image processing, 2nd ed. Upper Saddle River, NJ: Prentice Hall; 2002.
17. Imielinska C, Xin L, Sughrue M, Hagiwara E, Connolly ES Jr, D′Ambrosio A. Proceedings of CARS 2004. Computer Assisted Radiology and Surgery. June 2004:pp. 34-43 Elsevier-Verlag. Amsterdam, 2004. pp. 830-835.
18. Klotz. E, König, "perfusion measurements of the brain: using dynamic CT for the quantitative assessment of cerebral ischemia in acute stroke, European Journal of Radiology, 30:170–184, 1999.
19. Tomandl BF, Klotz E, Handschu R, et al., Comprehensive imaging of ischemic stroke with multisection CT", RadioGraphics, 23:565–592, 2003.